SUPPLEMENTARY INFORMATION

Manufacturing of Complex Diamond-Based Composite Structures via Laser Powder-Bed Fusion

Loic Constantin,[1,2,‡,] Nada Kraiem,[1,2,‡,] Zhipeng Wu,[1,‡,] Bai Cui,[3,] Jean-Luc Battaglia,[4,]

*Christian Garnier,[5,] Jean-François Silvain,[1,2,] * and, Yong Feng Lu,[1,] **

[1] Department of Electrical and Computer Engineering, University of Nebraska-Lincoln, Lincoln, NE, 68588, USA.

[2] CNRS, Univ. Bordeaux, Bordeaux INP, ICMCB, UMR 5026, F-33608 Pessac, France.

[3] Department of Mechanical and Materials Engineering, University of Nebraska-Lincoln, Lincoln, NE 68588-0526, USA.

[4] CNRS, University of Bordeaux, I2M, UMR 5295, F-33400 Talence, France

[5] LGP-ENIT-INPT, M2SP team, University of Toulouse, F-65016 Tarbes, France

1. Powders used for LPBF of Cu/D composite

Fig. S1a shows a scanning electron microscopy (SEM) micrograph of the original diamond (D) particles. As mentioned in the manuscript, the D particles were coated with a graded titanium oxide –carbide (TiO_2-TiC) layer to improve the wettability with molten copper (Cu), as displayed in **Fig. S1b**. Then, Cu and coated -D powders (**Fig. S1c - d**) were mixed at a concentration of 5 vol.% of the coated -D, as presented in **Fig. S1e - f**. Finally, the powder mixture was loaded into the SLM® 125 printer for laser powder-bed fusion (LPBF) manufacturing.

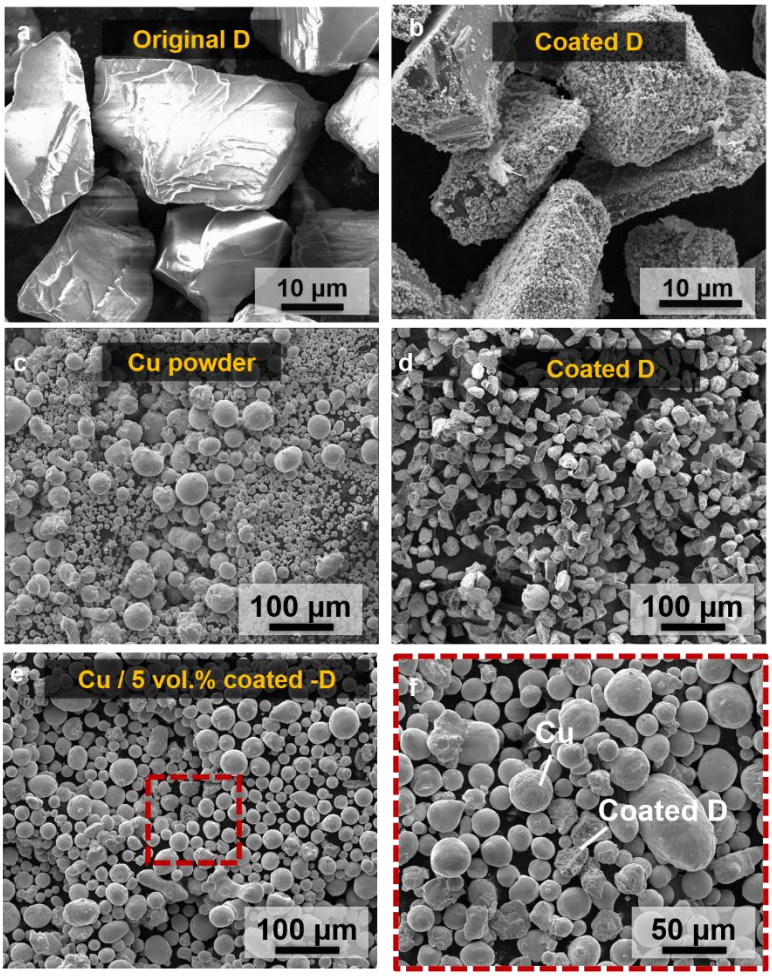

Fig. S1. (a) SEM micrographs of the original D powder, **(b)** coated -D powder with a TiO_2-TiC layer, **(c)** Cu powder, **(d)** coated -D powder, and **(e**, **f)** Cu/coated -D mixture.

2. The single-melting strategy

The common printing strategy is a single-melting one involving three-steps. **Fig. S2** illustrates the steps in a single-melting strategy. First, the recoater blade passes on the build plate to depose a composite powder (Cu and coated -D powders). Next, the laser selectively melts the powder into the desired shape. Finally, the build plate is lowered for the deposition of a new layer. By repeating the process, 3D structures are printed.

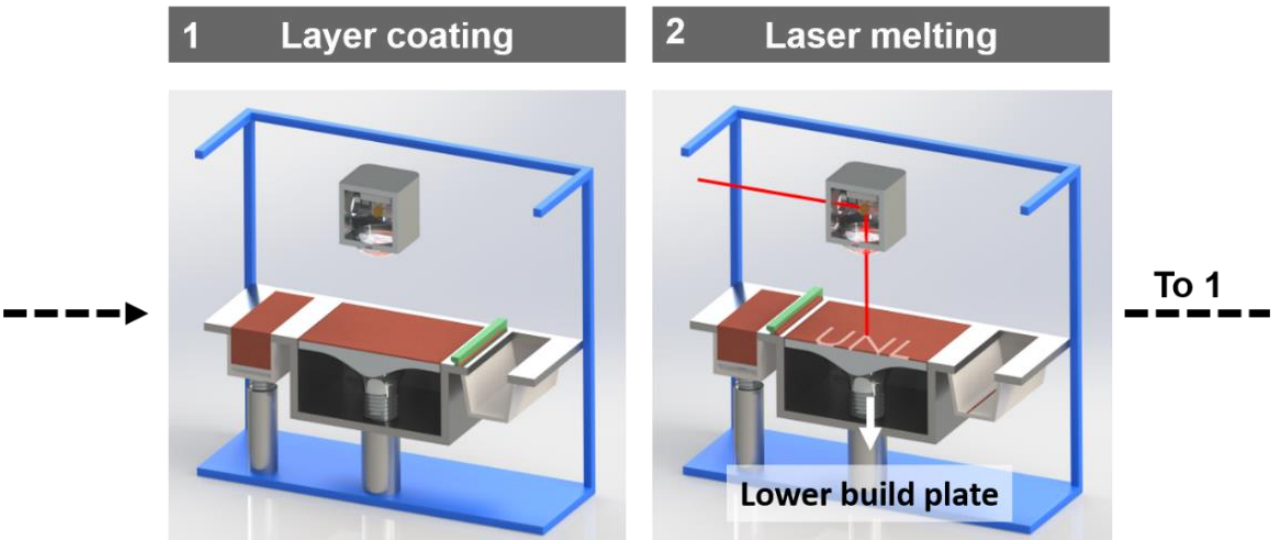

Fig. S2. Illustration of the steps involved in a single-melting strategy during LPBF.

3. Spatter ejection: Pure Cu vs. Cu/D powder beds

Fig. S3a is a photograph of the laser applied to a pure Cu powder bed. The laser power, scan speed, hatch distance, and layer thickness are 400 W, 400 mm/s, 0.12 mm, and 0.03 mm, respectively. As can be seen, a bright spot appears at the bed surface due to the metal evaporation and spatter ejection. **Fig. S3b** is a photograph of the laser matter-interaction on a Cu and D powder bed with the same printing parameters as used for the pure Cu bed. A significant difference in the metal vapor and spatter ejection is observed.

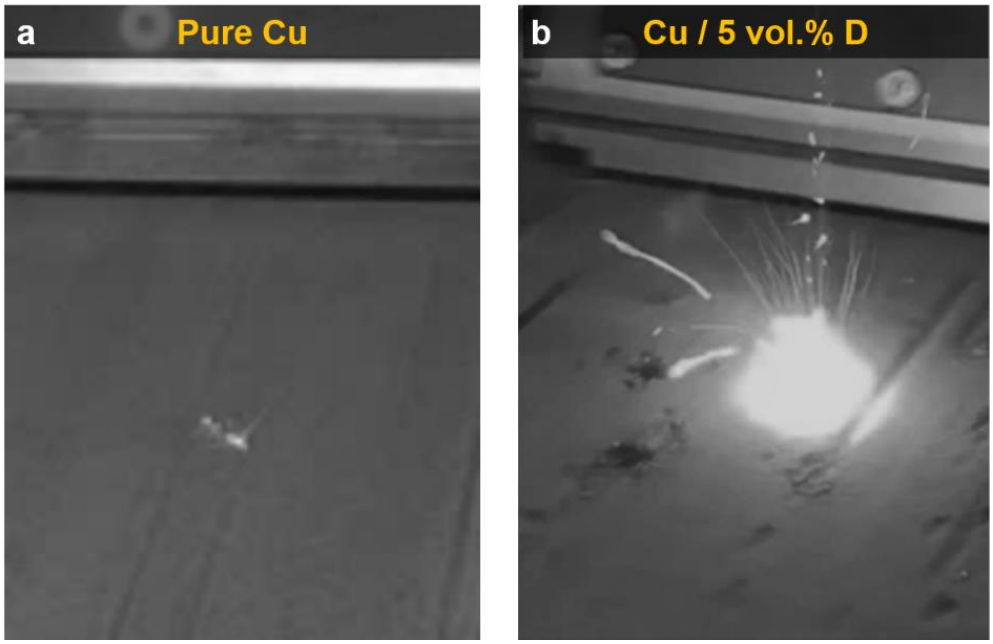

Fig. S3. (a) Photographs of the laser shining on a Cu powder bed, and **(b)** Cu/D powder bed for the same printing parameters (P = 400 W, s = 400 mm/s, h = 0.10 mm, LT = 0.03 mm).

4. Pictures of samples printed using the single-melting strategy

Fig. S4 shows photographs of the samples printed using the single-melting strategy. These photographs were used to create the two-dimensional (2D) maps in the manuscript **(Fig. 2e**).

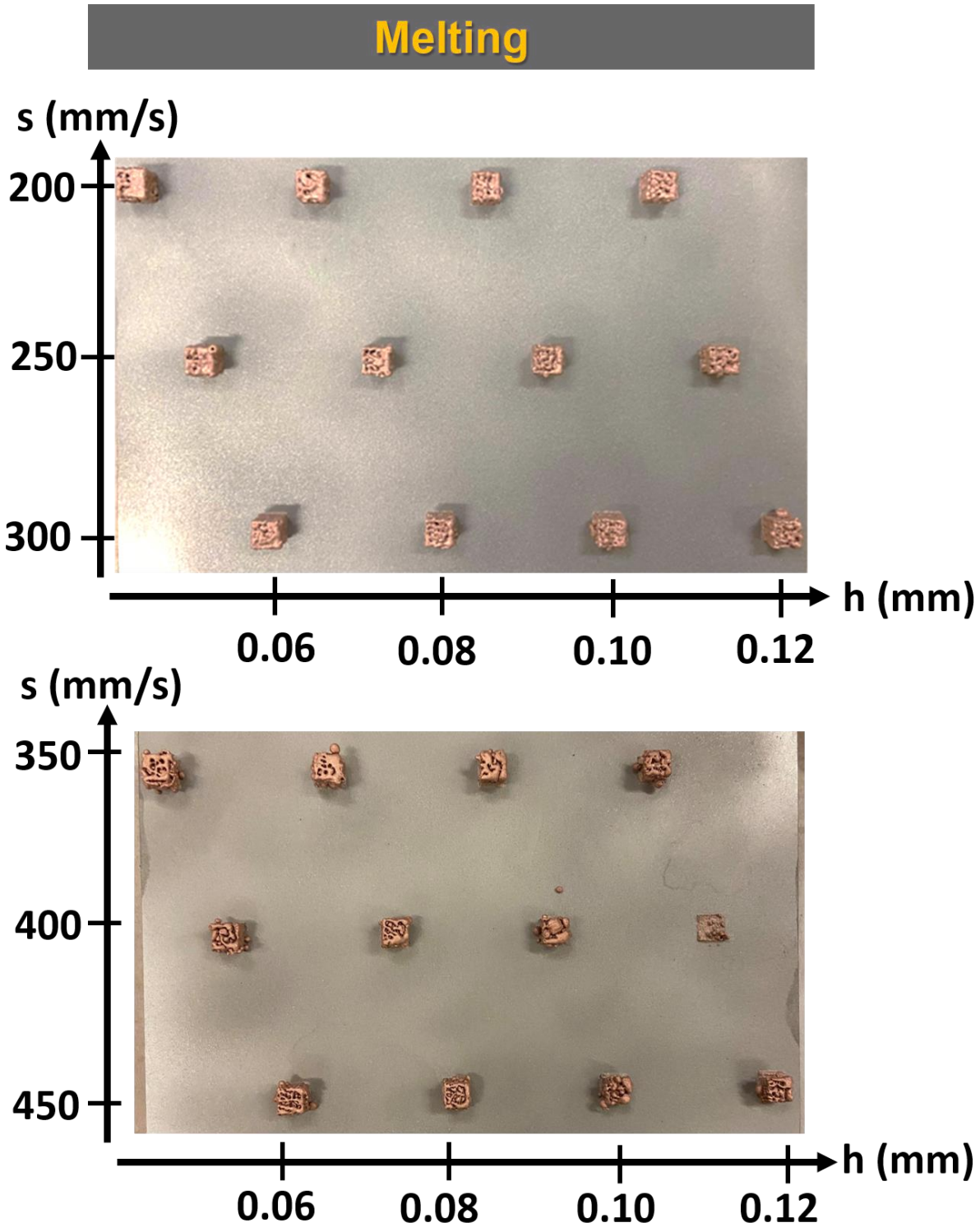

Fig. S4. Photographs of building Cu/D composites for scan speeds and hatch distances ranging from 200 to 400 mm/s and 0.06 to 0.12 mm, respectively, using the single-melting strategy.

5. Recoating and remelting strategies

The recoating strategy was employed to print Cu/D composites. This approach adds two steps to the process compared to the conventional single-melting one, as presented in **Fig. S5**. After the deposition of the first layer and laser melting, a second layer is deposited on the build plate without lowering the plate. Next, the laser is applied a second time to densify the powder. Finally, the plate is lowered, and the steps are then repeated to print a 3D structure.

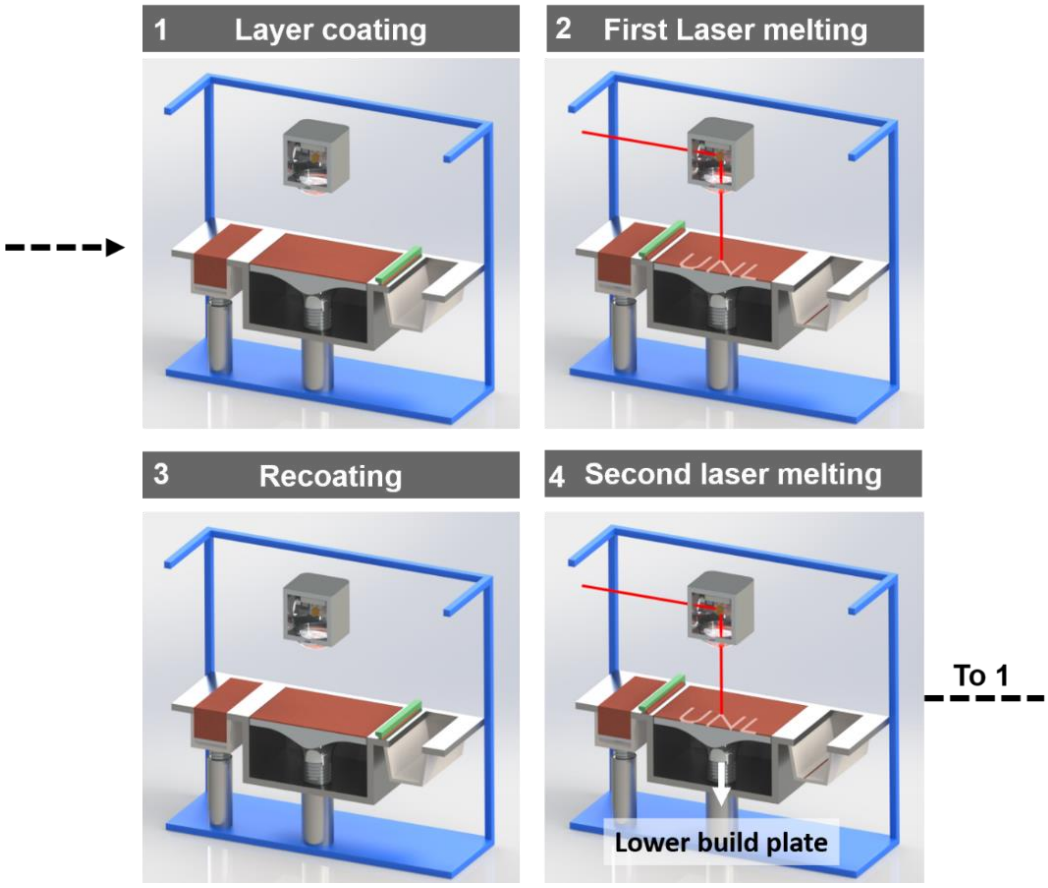

Figure S5. Illustration of the steps involved in the recoating strategy during LPBF.

The third approach studied in this work, involves remelting. As shown before, a layer is deposited on the build plate, and the laser melts the powder. Next, the laser is applied on the same layer a

second time. The build plate is then lowered. By repeating the process, the three-dimensional (3D) structure is printed via a remelting strategy, as shown in **Fig. S6**.

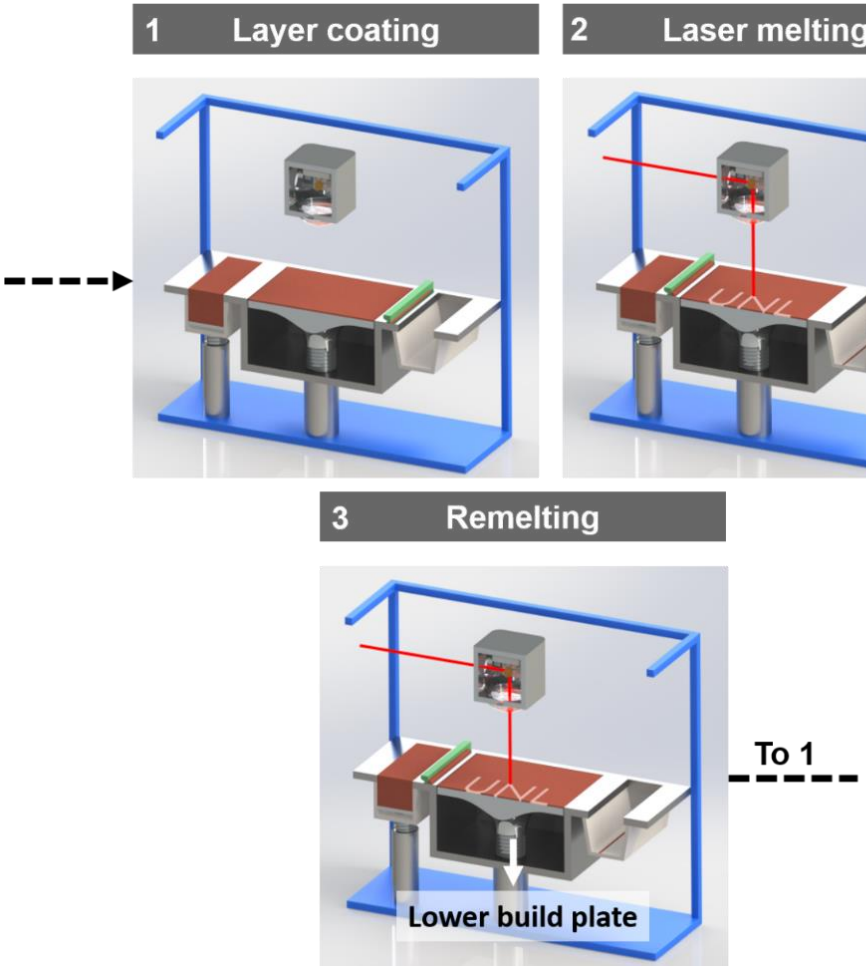

Figure S6. Illustration of the steps involves in a remelting strategy during LPBF.

6. Pictures of samples printed using the recoating and remelting strategies

Figs. S7 and **S8** consist of the photographs of samples printed using the recoating and remelting printing strategies. These photographs were used to create the 2D maps in the manuscript in **Fig. 3a - b**.

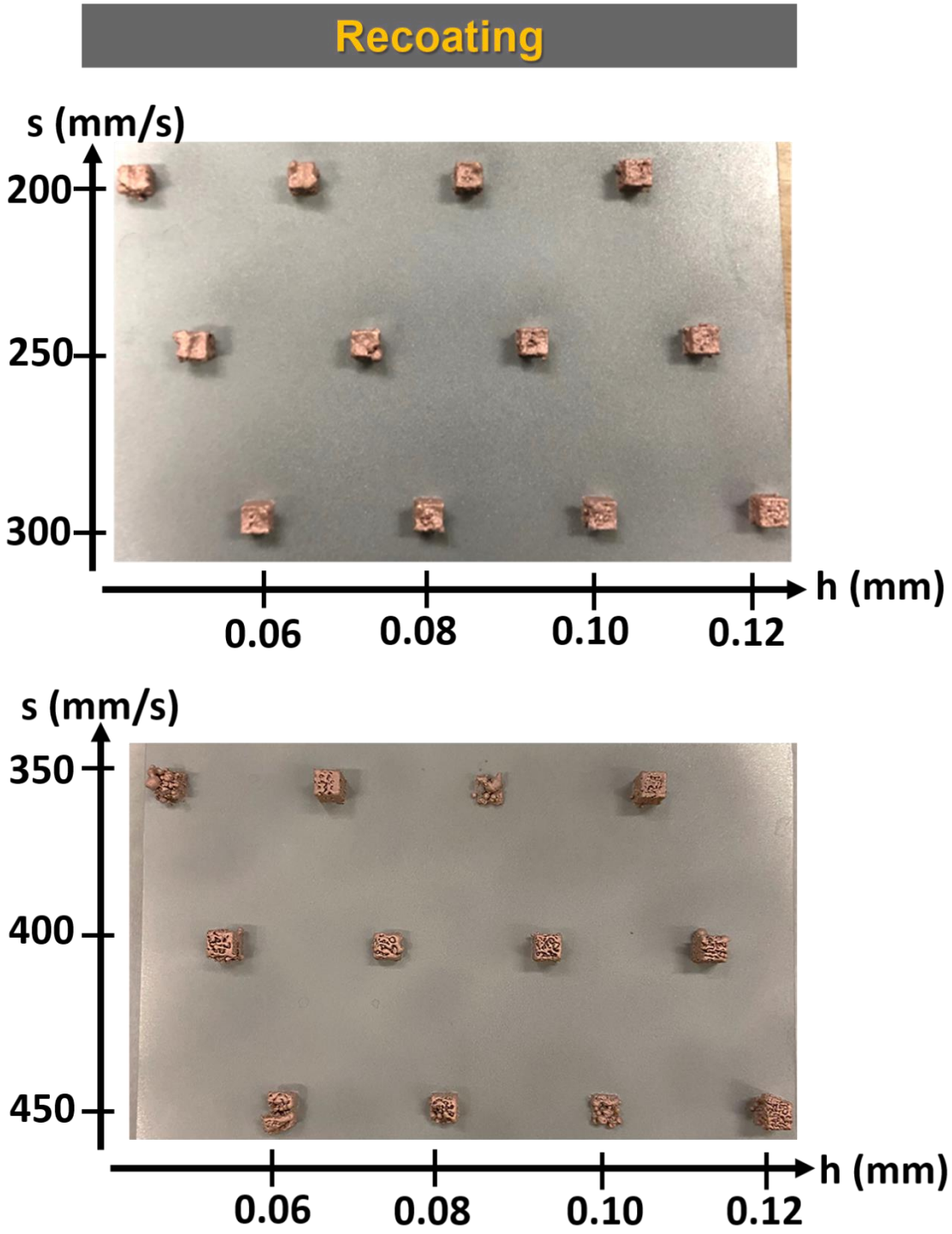

Fig. S7. Photographs of building Cu/D composites for scan speeds and hatch distances ranging from 200 to 400 mm/s and 0.06 to 0.12 mm, respectively, using the recoating strategy.

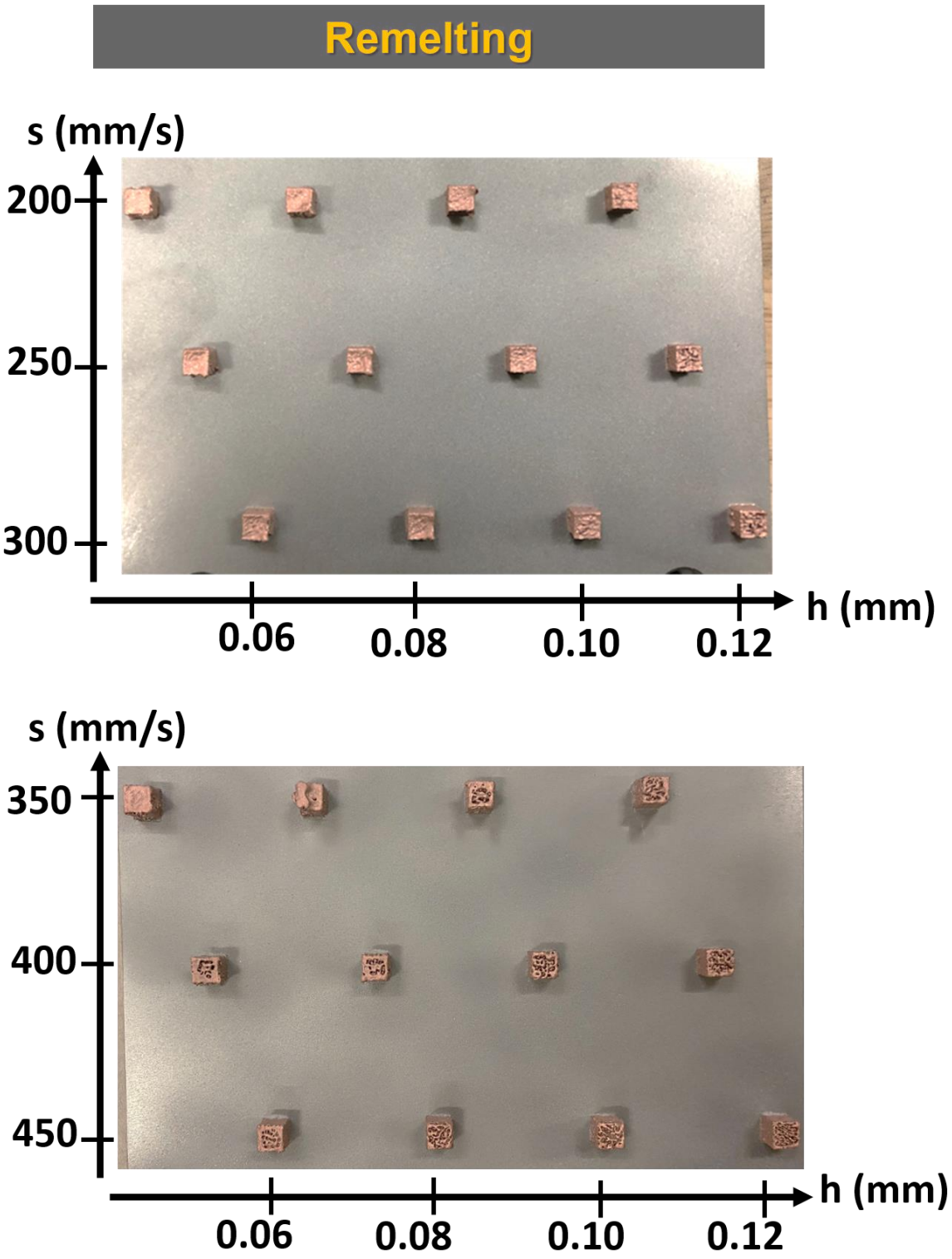

Fig. S8. Photographs of building Cu/D composites for scan speeds and hatch distances ranging from 200 to 400 mm/s and 0.06 to 0.12 mm, respectively, using the remelting strategy.

7. Surface roughness

The surface of the printed Cu-D cubes at a scan speed and hatch distance of 250 mm/s and 0.1 mm, respectively, were analyzed using an optical surface profiler (Zygo NewView 8000). **Fig S9a - c** shows the printed cubes' surface using the melting, recoating, and remelting strategies. The average surface roughness is plotted in **Fig S9d**. It can be observed that the average roughness is 134 µm with a melting strategy. The roughness decreases to 85 µm and further decrease down to 25 µm with a remelting strategy.

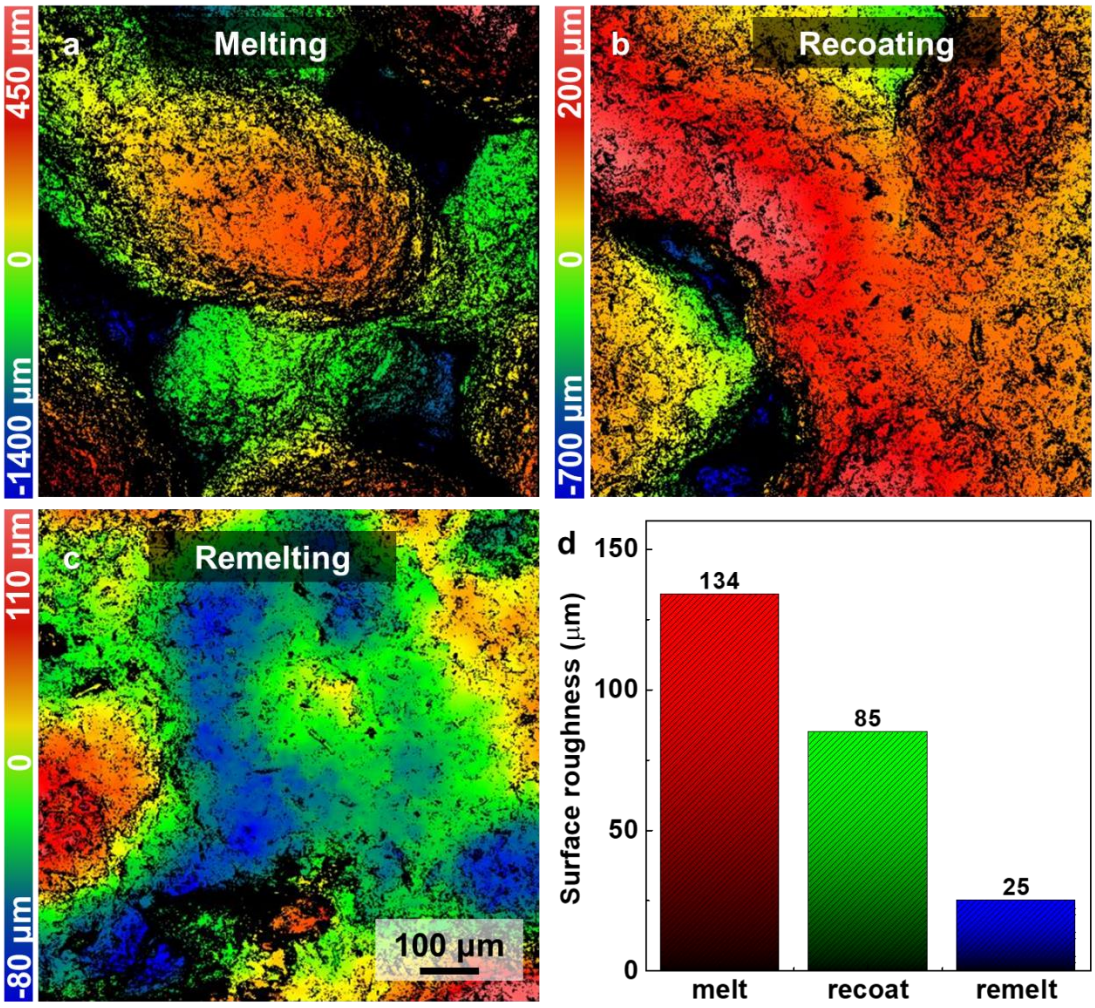

Fig. S9. Surface mapping of Cu/D composites printed with **(a)** melting, **(b)** recoating, and **(c)** remelting strategies. **(d)** A plot of the surface roughness vs. printing strategies.

8. Molten pool profile

The molten pool profiles of different printing strategies were analyzed on the section of the printed cubes at a scan speed and hatch distance of 250 mm/s and 0.1 mm, respectively. For that, the samples were etched into a nitric acid/ water solution (50:50) for 30 s. **Fig S10 a-c** show optical microscope images of the samples' section where the molten pool can be observed. **Fig S10 d – f** show SEM micrographs of the molten pool near the samples' surface.

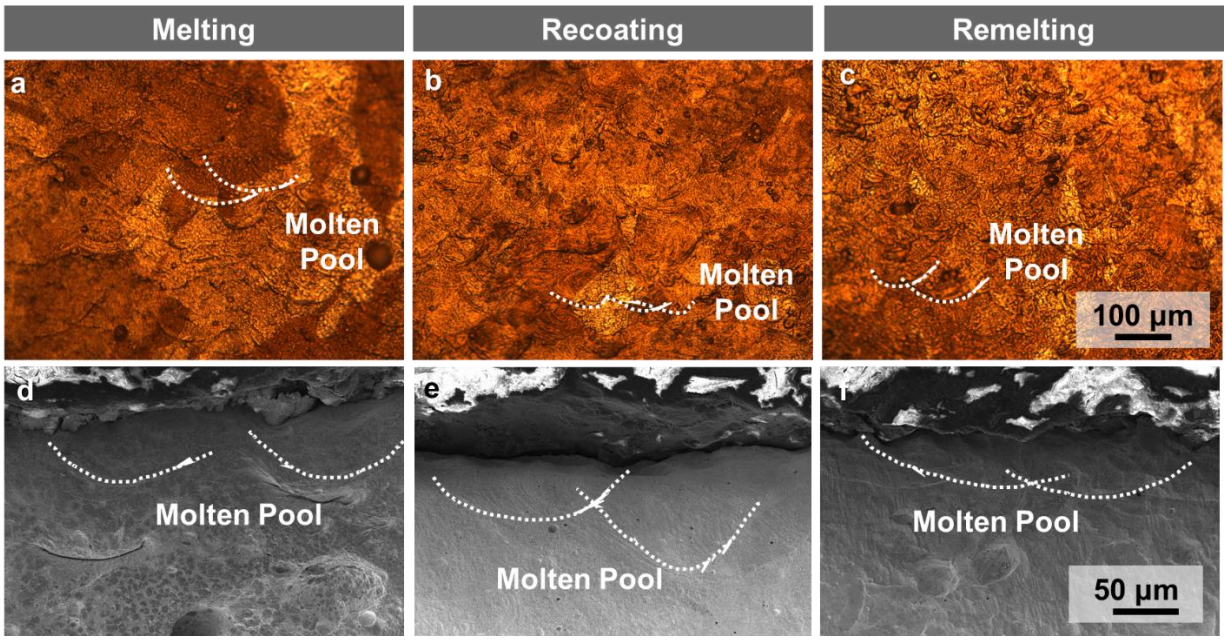

Fig. S10. Optical images of molten pool profile for **(a)** melting, **(b)** recoating, and **(c)** remelting strategies. SEM micrographs of molten pool profile for **(d)** melting, **(e)** recoating, and **(f)** remelting strategies.

9. Thermal conductivity measurement

The periodic photothermal radiometry (PPTR) technique was used to measure the thermal diffusivity (TD) of the Cu/D composite materials printed. The setup is equipped with an Nd: YAG

laser (Coherent MATRIX Q-switched diode-pumped laser, λ = 1064 nm) that delivers a a finite pulse width excitation by emitting a N_p-pulse train at frequency f_p=30 KHz (maximum rms power of 10 W). Each pulse duration is equal to 40 ns. The pulse width is thereby $\Delta t_{burst}=N_p/f_p$. The pulse train is repeated with frequency f_{exc}=4Hz using a function generator. The laser beam (radius 0.55 mm) is directly focused on the sample. An infrared (IR) detector (Teledyne Judson Technologies J15D12) is used to monitor the temperature change at the rear face of the sample. Also, a photodiode is set to trigger the acquisition after each pulse train. An averaging process is performed throughout repetition period $T_R=1/f_p$ considering N_s cycles that allows the signal-to-noise ratio of the detector's response to be increased and to reduce the noise standard deviation of temperature values by $\sqrt{N_s}$. The TD of the sample is identified by minimizing the gap between the experimental response and the theoretical one calculated using an analytical solution of the heat transfer of material. The minimization is achieved by implementing a nonlinear least square algorithm (the Levenberg-Marquardt technique).

Fig S9a-c presents the experimental data of the TD measurement using the PPTR method. A close correlation between the experimental curve and the model can be observed in **Fig. S9** with a low residual signal. The TDs measured for the melted, recoated and remelted samples were 68.48, 95.04, and 101.331 mm^2/s. The thermal diffusivity was converted into thermal conductivity (TC) using the following equation:

$$k(T) = a(T) \times C_p(T) \times \rho(T), \qquad (1)$$

where k is the TC (W/m.K), a is the TD (mm^2/s), ρ is the density (g/cm^3), and C_p is the heat capacity of the sample (J/Kg.K). The C_p of the diamond, TiC, and Cu used in this study are 630, 190, and 392 J/Kg.K, respectively, leading to a thermal conductivity of 236, 327, and 349 W/m.K, respectively, for the samples printed.

a

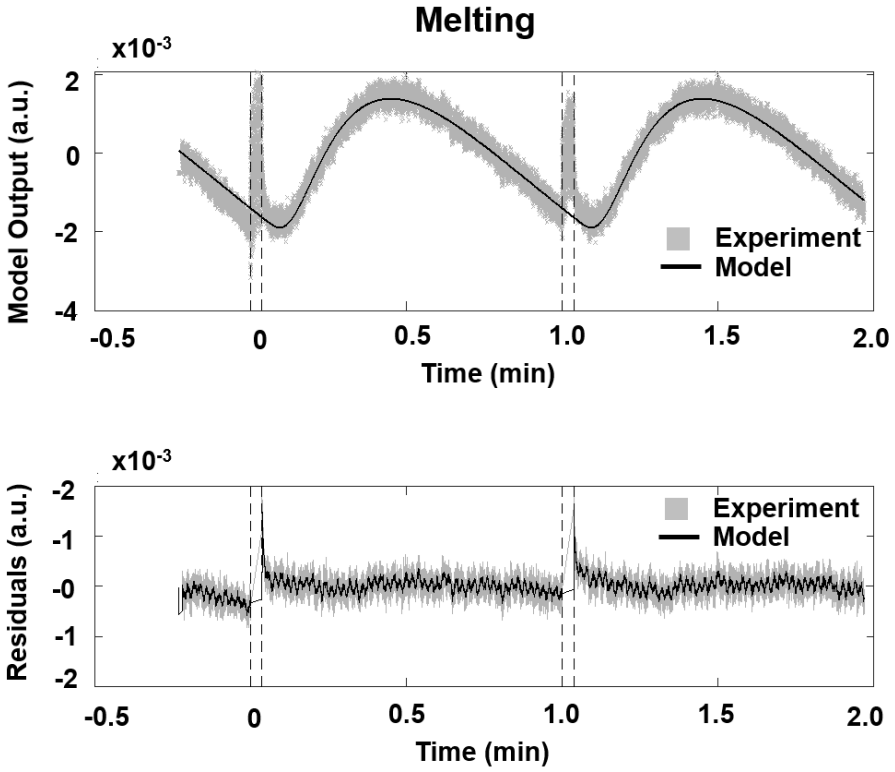
Melting
x10-3
Model Output (a.u.)
Experiment
Model
Time (min)
x10-3
Residuals (a.u.)
Experiment
Model
Time (min)

b

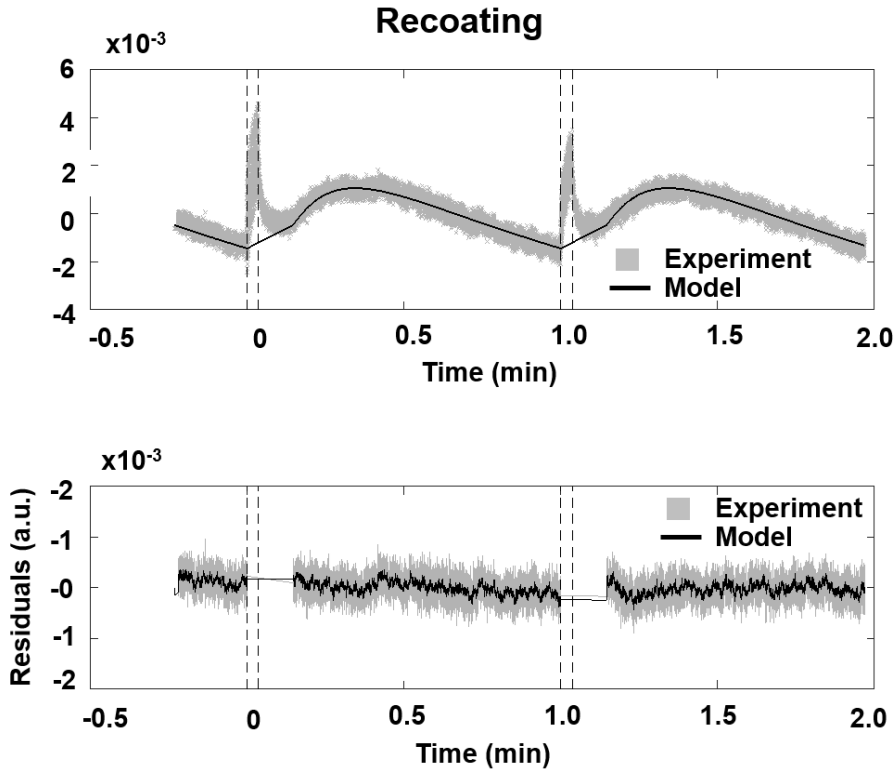
Recoating
x10-3
Experiment
Model
Time (min)
x10-3
Residuals (a.u.)
Experiment
Model
Time (min)

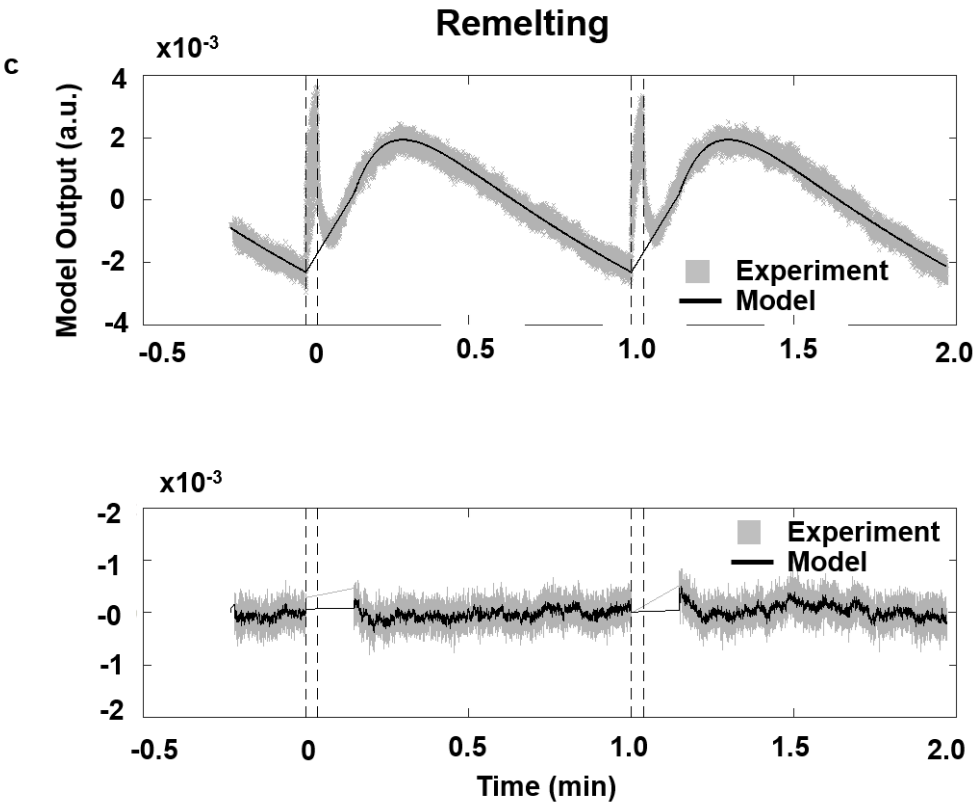

Fig. S11. (a) Plots of the measured and theoretical temperature with the identified thermal diffusivity vs. time and residuals vs. time for a Cu/D printed with a single-melting strategy, **(b)** recoating, and **(c)** remelting.